

## Article

# Numerical Analysis of Crashworthiness on Electric Vehicle's Battery Case with Auxetic Structure

Liviu I. Scurtu , Ioan Szabo \* and Marius Gheres

Automotive Engineering and Transport Department, Faculty of Automotive, Mechatronics and Mechanical Engineering, Technical University of Cluj-Napoca, 103-105 Muncii Avenue, 400641 Cluj-Napoca, Romania; liviu.scurtu@auto.utcluj.ro (L.I.S.); marius.gheres@auto.utcluj.ro (M.G.)

\* Correspondence: ioan.szabo@auto.utcluj.ro

**Abstract:** Due to the reduction in pollutant emissions, the number of electric vehicles has experienced rapid growth in worldwide traffic. Vehicles equipped with batteries represent a greater danger of explosion and fire in the case of traffic accidents, which is why new protective systems and devices have been designed to improve impact safety. Through their design and construction, auxetic structures can ensure the efficient dissipation of impact energy, reducing the risk of battery damage and maintaining the safety of vehicle occupants. In this paper, we analyze the crashworthiness performance of a battery case equipped with an energy absorber with a particular shape based on a re-entrant auxetic model. Simulations were performed at a velocity of 10 m/s and applied to the battery case with a rigid impact pole, a configuration justified by most accidents occurring at a low velocity. The results highlight that by using auxetic structures in the construction of the battery case, the impact can be mitigated by the improved energy absorber placed around the battery case, which leads to a decrease in the number of damaged cells by up to 35.2%. In addition, the mass of the improved energy absorbers is lower than that of the base structure.

**Keywords:** electric vehicle; battery; impact; auxetic structure; re-entrant auxetic structure; mechanical stresses



**Citation:** Scurtu, L.I.; Szabo, I.; Gheres, M. Numerical Analysis of Crashworthiness on Electric Vehicle's Battery Case with Auxetic Structure. *Energies* **2023**, *16*, 5849. <https://doi.org/10.3390/en16155849>

Academic Editor: Quanqing Yu

Received: 29 June 2023

Revised: 25 July 2023

Accepted: 4 August 2023

Published: 7 August 2023



**Copyright:** © 2023 by the authors. Licensee MDPI, Basel, Switzerland. This article is an open access article distributed under the terms and conditions of the Creative Commons Attribution (CC BY) license (<https://creativecommons.org/licenses/by/4.0/>).

## 1. Introduction

As the market for electric vehicles continues to grow and prices continue to fall, people will have easier access to purchase electric vehicles. Several factors influence the rise of green cars, including government incentives, awareness of environmental issues, falling battery costs, and other developments. Electric vehicles, which produce no emissions, help improve air quality and reduce emissions of gases that contribute to global warming. With the ongoing advancements in fuel cell technology, the use of vehicle batteries is expected to escalate further [1,2]. The integration of batteries in fuel cell vehicles has the potential to enhance their range, performance, and efficiency, thereby rendering them a more feasible alternative for consumers [3].

Internal combustion engine (ICE)-powered vehicles have long been a significant source of air pollution. Their reliance on fossil fuels such as petroleum and diesel contributes to air pollution by emitting carbon dioxide (CO<sub>2</sub>), nitrogen oxides (NO<sub>x</sub>), particulate matter (PM), and volatile organic compounds (VOCs). These emissions negatively impact both human health and the environment. They lead to air contamination, the formation of haze, respiratory diseases, and climate change on a global scale [4].

Conventional vehicles negatively impact the environment, but electric vehicles offer a suitable solution. Electric vehicles (EVs) are powered by rechargeable batteries and electric motors, unlike ICE vehicles, eliminating exhaust emissions and decreasing reliance on fossil fuels. We can substantially reduce pollution through electrification, working toward a greener, healthier future [5,6].

Due to their high energy density and extended life cycle, lithium-ion batteries are commonly utilized in electric vehicles. With the growth of electric vehicles, combustion and explosion accidents have been observed [4–7]. The battery case is examined under dynamic loading to investigate the safety characteristics of lithium-ion batteries under dynamic shock conditions. There are three main categories of ground collisions for electric vehicles: (1) a battery case is pierced by sharp objects on the road, (2) a foreign object is trapped between the road surface and the battery case, or (3) a battery case is directly struck or ejected by foreign objects. Batteries can be subjected to three-point deformation, extrusion, needling, and drop-weight tests for mechanical safety. The intrinsic safety characteristics of the battery can be examined using three-point bending and static extrusion tests, whereas drop-weight impact tests more accurately simulate a thermal runaway [8–11].

However, it is challenging to develop BEV design solutions to pertinent issues. Increasing the size and capacity of the onboard battery cell and developing technologies to expedite battery recharging are necessary solutions. In their study, Belingardi et al. presented battery cell impact protection by focusing on side impacts against another vehicle and solid obstacles. Three solutions for reinforcement of the lateral rocker were investigated. The results of a finite element (FE) analysis demonstrate the efficacy of the various solutions and the significance of selecting the appropriate wall thickness [12].

Auxetic models are used in a variety of applications, including automotive [10–14], energy absorption [15,16], medical [17–19], aerospace [20], ballistic protection materials [21–23], civil engineering [24,25], and sports [26,27]. Luo C. et al. realized a comprehensive review of the design and fabrication of auxetic tube structures, including various cellular auxetic tubes, nonporous and porous auxetic tubes, and auxetic nanotubes, as well as macro and micro auxetic tubes [28]. A detailed description of the mechanical properties of auxetic structures, such as impact energy absorption, synclastic behavior, and bending performance, was presented. In addition, several potential applications, such as energy absorption devices, angioplasty and stents for medical applications, fasteners, and nails, were summarized. Although recent advances in fabrication and 3D printing technologies could be used to develop auxetic structures, the high fabrication cost and unstable mechanical behavior may still prevent widespread application. Z. Wang et al. [29] classified and analyzed auxetic mechanical metamaterials (AMMs) according to their structural characteristics and deformation mechanisms. In addition, their properties, including shear strength, penetration resistance, rupture strength, synclastic behavior, energy absorption of the structure, and variable permeability, were investigated. The summary of manufacturing methods and materials included additive, subtractive, and other methods. The study of AMMs has made significant progress, but numerous obstacles and limitations must be surmounted. In addition, the high cost of production severely restricts the mass production and applications of AMMs. Lastly, polyvalent application fields based on the characteristics of AMMs have not yet been rigorously designed or studied.

However, in extensive research, F. E. Carakapurwa et al. attempted to reduce the risk of battery damage by optimizing the design for optimum specific energy absorption (SEA) [10]. A cell structure with an auxetic shape for the negative Poisson ratio was used to obtain excellent energy absorption results. A crash scenario was created to determine the SEA value of diverse design samples using the finite element method (FEM). Machine learning (ML) was used to anticipate the design that yielded the highest SEA. The optimal layout was determined using an ANN and NSGA-II. Sorting Genetic Algorithm II (NSGA-II) was used to optimize an aluminum Al 6061 T6 star-shaped auxetic structure with a thickness of 2.95 mm, an inner spacing of 5.557 mm, and a corner angle of 56.82 degrees. The improved model had a 12-fold greater SEA than the baseline model and a 1 mm-thick re-entrant auxetic structure made of carbon steel. The optimized model validated by FEM simulation showed a deviation between the ANN-NSGA prediction and FEM analysis of 6.7%, indicating that the improved model is valid. Further research including additional investigation of machine learning algorithms considering thermal dissipation for optimization is encouraged to expand the data training [13].

Gunaydin et al. [30] studied chiral lattice structures and compressed them flatwise between two rigid plates using a quasistatic loading procedure. At the same time, the crosshead velocity was constant at 10 mm/min. The compression test was conducted using an Instron Universal Testing Machine (model 5890) with a 100 kN loading capacity, and load–displacement diagrams were drawn. Four specimens were tested during quasistatic crushing experiments, and a mass scale was applied to reduce the experimental time. ABAQUS-Explicit was used for the FEM analysis, and a study of chiral auxetic lattices was also utilized to validate the FEM results. Consequently, chiral auxetic structures have a better impact energy absorption capacity than chiral hexagonal, antitetrachiral, and re-entrant auxetic lattice structures. The impact energy absorption capacity of chiral hexagonal auxetic lattices is superior to that of re-entrant and antitetrachiral lattices, and the SEA value of re-entrant and antitetrachiral lattices under quasistatic load with a constant velocity of 10 mm/min is nearly identical.

Crashworthiness is a measure of the plastic deformation of vehicle structures, such as collisions and energy-absorbing member structures like bumpers and crash boxes. Our aim was to thoroughly understand crash box studies by examining the various approaches and facets of crash box research conducted on automobiles. The primary objective of such research is to protect individuals from unfortunate occurrences such as impacts, accidents, and collisions. The aim of this study was to determine how a crash box's design or configuration impacts its crash performance. Thin-walled structures are commonly used as impact boxes, but numerous other approaches and configurations have been proposed. Welding and adhesives are examples of joining techniques that contribute to the complexity of design. Computational analysis is utilized alongside experimental work for correlation purposes, but model improvement is advised for accident prediction analysis to obtain a reliable analytical model [31].

In their research, Biharta et al. designed and optimized a sandwich structure based on an auxetic design to shield the pouch battery model of electric vehicles subjected to ground impact loads [29]. The interior of the layer structure was completed with optimized auxetic structure cells that were lengthened by 200%, arranged in  $11 \times 11 \times 1$  cells, for a total dimension and mass of  $189 \times 189 \times 12$  mm and 0.75 kg, respectively. The improved sandwich structure demonstrates that battery cells can be secured from ground impact loads up to a maximum deformation of 1.92 mm, which is below the battery failure deformation threshold. During compression loading in a numerical simulation, the optimized model's specific energy absorbed emission ranged between 38.75 and 45.03 kJ/kg, with a mean of 42.19 kJ/kg. The optimal cell configuration is represented the second case, in which the optimized cell structure was enlarged to 200% in length and arranged in  $5 \times 5 \times 1$  cells, yielding a volume of 168,488.23 mm<sup>3</sup> and a total mass of 0.75 kg. The results show that the maximum battery deformation is 1.92 mm, which is less than the 2.9 mm deformation threshold for battery failure [32].

Furthermore, Biharta et al. investigated a new design of sandwich-based auxetic honeycomb structures to shield pouch battery cells for electric vehicles subjected to axial impact loads [33]. The techniques for the optimization of structures they used included the Non-Dominated Sorting Genetic Algorithm Type II (NSGA-II), the Technique for Order of Preference by Similarity to Ideal Solution (TOPSIS), and an artificial neural network (ANN). The optimized design had dimensions of 6 mm in length, 4.2 mm in width, and 0.6 mm in cross-sectional thickness, with a single layer. The optimized design had an SEA of 47,997.84 J and was able to maintain a maximal von Mises stress of 43.16 MPa on the battery. The auxetic structure absorbed 425.15 of 917.13 J of internal energy during impact. The reaction of the entire structure during vehicle impact conformed to classical crash mechanics, with a zero-crossing time of 1.39 milliseconds, a rebound velocity of 2.5 m per second, and a maximum crushing force of 40.5 kN.

Wang, et al. [34] reported a novel battery pack that consists of a non-modular battery pack (CTP) and two negative-Poisson-ratio (NPR) tubular structures. On both sides of the CTP, an anti-collision block and radiator are installed to satisfy the crashworthiness and

heat dissipation requirements. The optimized NPR-CTP system was determined using a multiple-objective optimization method. The initial NPR-CTP system had superior crash-worthiness and thermal dissipation compared to other CTP systems, and the optimized system's overall performance was significantly enhanced. The performance of the NPR-CTP system was analyzed using the Pareto method in conjunction with the radial basis function (PSO-RBF) and the third-generation non-dominant ranking genetic algorithm (NSGAIII). The results demonstrated that the NPR-CTP system achieved superior overall performance (structural safety and thermal dissipation) compared to conventional hollow and PPR tubular structures. The optimization objectives were maximum acceleration, maximum intrusion displacement ( $S_{max}$ ), specific energy absorption, and maximum temperature of the battery ( $T_{max}$ ), and the NBI method determined the optimized scheme from the Pareto solution set. The optimized NPR-CTP system had a lower  $S_{max}$  and a smaller  $T_{max}$  than the initial system, and its  $A_{cc}$  was 24.083 g (26.22%) less than that of the initial system, which indicates that the structural safety performance and the ability to dissipate heat were effectively enhanced by multi-objective optimization. Based on the results reported above, auxetic structures are excellent energy-dissipating materials because of their negative Poisson ratio, which yields improved energy absorption. Considering the broad applicability of auxetic structures, they can also be included to protect the batteries used in electric vehicles. As the number of electric vehicles is constantly increasing, a corresponding increase in accidents can be expected. The crucial role of the auxetic structures included in the battery case is to protect and absorb/attenuate part of the shocks resulting from a car accident. To the best of our knowledge, auxetic elements in this configuration have not been used for energy absorbers in the battery case of an electric vehicle.

Considering that current research on mechanical stresses (impact) on electric vehicle battery cases has been carried out for classic design forms (box type/parallelepipedal), this paper proposes an innovative approach to battery case design. The novelty of the topic studied in this article also lies in the fact that we have not encountered this approach in the studied literature. By implementing auxetic structures in the construction of a battery case, we managed to reduce the frontal impact energy and transmit it along the box (housing/case).

This study presents the possibilities of implementing some auxetic structures in the construction of the battery case of electric vehicles designed to dissipate the impact energy in an accident and reduce the damage to the battery components (cells). The main purpose of this study is to demonstrate the use of auxetic structures in mechanical structures to dissipate mechanical shock in the case of impact using computerized numerical analysis methods. A battery module consisting of 240 cylindrical cells (Li-Ion18650 type) was created, and battery case was designed for six different impact study cases (three different cases of geometric dimensions for the use of solid cylindrical structures and the use of auxetic cylindrical structures). The preprocessing stage involved the discretization of the models and the creation of loading cases using HyperMesh software. The explicit Radioss solver was used to calculate the numerical impact between the battery case and the pole, with the results displayed in HyperView.

## 2. Materials and Methods

Predictive behavior analysis of the new auxetic structure using the finite element method represents the aim of this study. The main steps of the research process are presented in Figure 1. Considering other research in the field, the effect of implementing some auxetic structures in the construction of a battery case should be investigated with reference to the impact between the battery and a rigid pole.

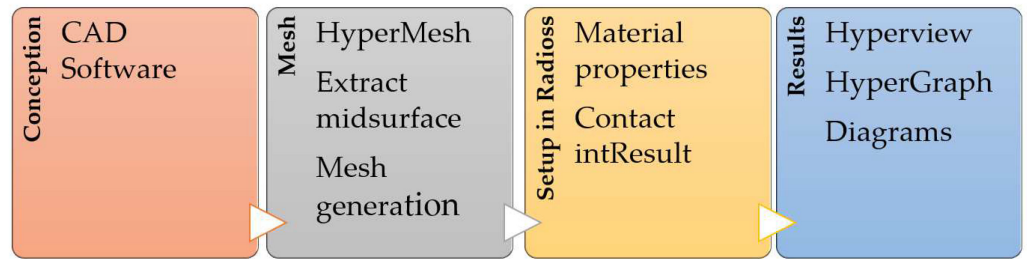


Figure 1. Flow chart of the numerical analysis process.

The re-entrant cutout geometry was practiced on a cylindrical surface to improve mechanical behavior. During the impact, the auxetic cutout absorbs the impact energy, increasing the protection of the battery cells inside the pack. Another strong point of using an auxetic structure is the decrease in mass. Six simulation cases were performed: three simulation cases with the base cylindrical surface as an energy absorber and another three cases with an auxetic structure. All simulation cases were analyzed under the working conditions of the base geometry. The cylindrical thickness of the re-entrant unit cell was 1.5 mm for all cases of analysis. All assembly parts were built using 3D modeling in SolidWorks software. A cylindrical surface was achieved after folding the planar surface, with re-entrant cells like those shown in the model in Figure 2 for three analysis cases. Figure 3 presents the developed surface and dimensions of the auxetic elements included on the cylindrical surface for 24 mm.

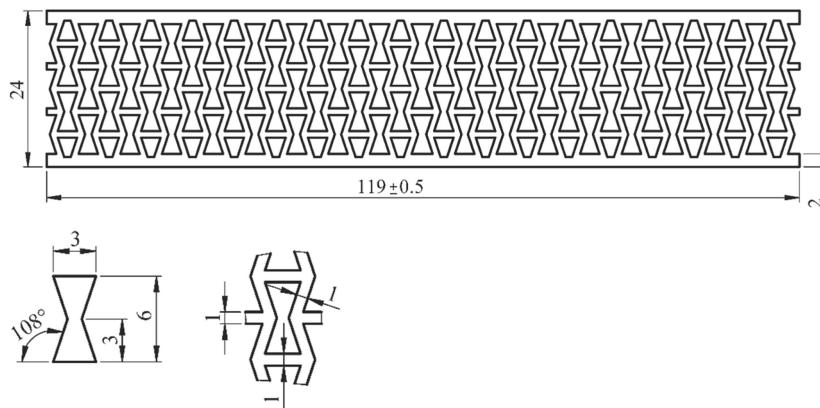


Figure 2. Developed surface and geometric details of the cylindrical cell of the re-entrant unit.

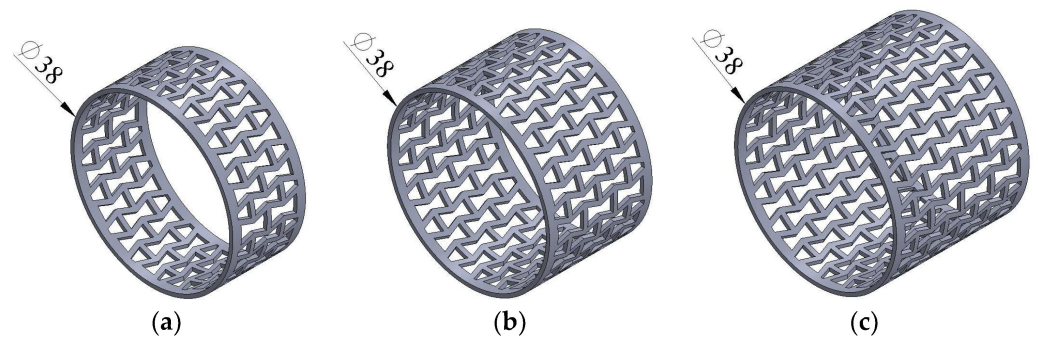
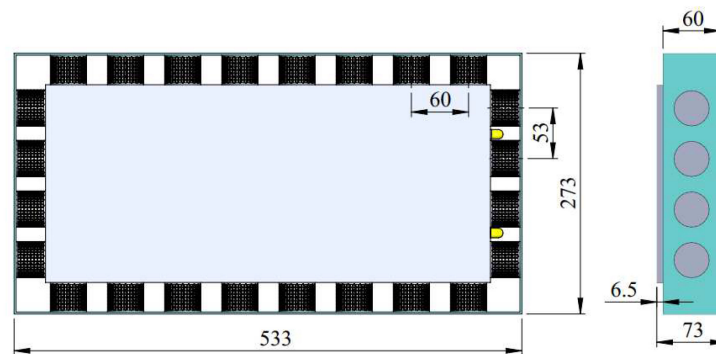
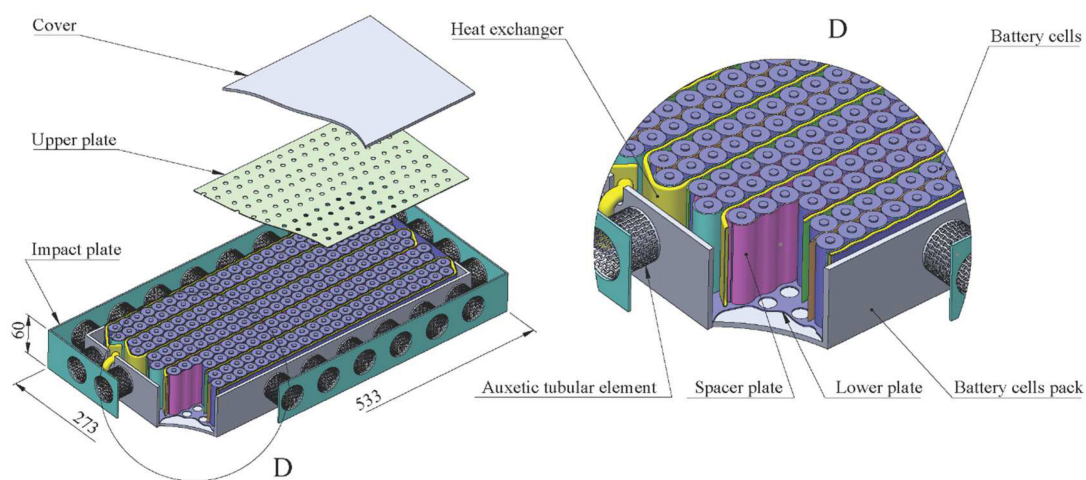


Figure 3. The re-entrant auxetic cylindrical models used in simulation (length: (a) 17 mm, (b) 24 mm, and (c) 31 mm).

The battery case assembly equipped with auxetic structures is shown in Figure 4, with the energy absorber elements placed perpendicularly around the battery pack (arranged as shown and a detailed view (D) of the auxetic structure is presented in Figure 5).



**Figure 4.** Geometric dimensions and top and side views of the battery pack model.



**Figure 5.** The design and components of the battery pack.

The current configuration of the battery pack consists of 240 individual 18,650-type Li-ion cells positioned inside the box, which is fixed to the lower and upper plates. A thermal management system was also considered, with cells between the heat exchanger plates and spacers (by ABS) placed between the rows of batteries to protect the cells. The external surface of the impact plate is perforated on the re-entrant unit cells, considering that area does not increase the safety of the battery cells during impact. The mass of the impact plate also decreases.

The finite element (FE) configuration presented in Figure 6 was created to simulate the behavior and distribution of mechanical stresses that appear in the structure of the battery module in the case of impact with a rigid steel pole with a diameter of 250 mm.

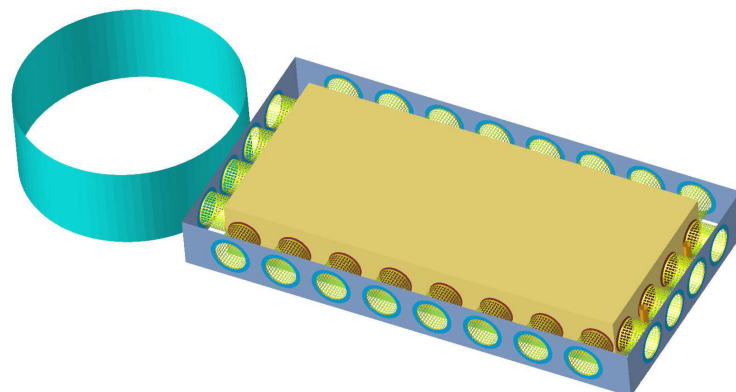


**Figure 6.** FE initial setup of the battery case impact simulation.

This section presents the necessary steps to create the finite element model for each assembly simulation load case. All components are discretized in shell, triangular, and rectangular finite elements. The essential cylindrical elements are named as follows: CYL1, CYL2, and CYL3 correspond to lengths of 17, 24, and 31 mm, respectively, and the perforated cylindrical elements with the re-entrant auxetic shape are named AUX1, AUX2, and AUX3 (Table 1). The base cylindrical cells are meshed into quad shell elements, and the re-entrant cylindrical cells are mixed into tria and quad elements. The target length of the energy absorber elements is 1 mm.

**Table 1.** Mass and elements of the energy absorber.

	CYL1	AUX1	CYL2	AUX2	CYL3	AUX3
Shell elements (1.5 mm thick)	48,144	28,968	67,968	38,616	87,792	48,216
Mass (kg)	0.1934	0.1081	0.2731	0.1455	0.3527	0.1821

Table 2 presents the quality criteria of the discretization process for each battery pack part. The data were imported into HyperMesh and meshed into finite elements. An optimal quality criterion was applied to each component of the cell. A finite element model and the crash scenario were created, including the components' contact, properties, and initial velocity with mechanical structural characteristics. The utilized contact interface was TYPE7, which assures permanent contact between the model's surfaces. Due to the difficulty of the calculations, a wall thickness of 0.8 mm was chosen to ensure appropriate battery cell behavior. Spacer plate parts placed between cells were made from ABS material with elastic–plastic behavior and characteristics assigned by an M36\_PLAS\_TAB card. The relationship between the stress and strain of the material behavior is given by the value of the strain in the range of 0–16 and the stress value in the range of 1–17.

**Table 2.** Mass and elements of the auxetic structure.

	Cover	Battery Pack	Upper Plate	Lower Plate	Heat Exchanger	Spacer Plates	Battery Cells	Impact Plate
FE element length (mm)	1	1	2	2	3	4	2	1
Thickness (mm)	4.0	4.0	1.0	1.0	0.4	1.0	0.8	2.0
Tria and Quad Shell	77,526	142,414	19,873	15,512	42,674	30,608	237,531	52,536
Mass (kg)	1.1320	1.8910	0.2303	0.1753	0.3999	0.5761	2.0030	0.3830

The materials' properties are reported in Table 3, with M2\_PLAS\_JOHN\_ZERIL as a nonlinear behavior material type designated for the components. This material is an isotropic elastic–plastic that replicates internal stresses as a function of strain and strength. All components of this evaluation were meshed into mixed shell elements with predefined properties of type P1\_SHELL. In the Radioss 2022 explicit solver environment, Altair HyperMesh software was used for the preparatory phase. Furthermore, the simulation results were interpreted using the HyperView and HyperGraph modules of the HyperWorks software package.

**Table 3.** Aluminum alloy 6063–T6 mechanical properties.

	Value	UM
Initial density	$2.7 \times 10^{-6}$	kg/mm <sup>3</sup>
Young's modulus	70	GPa
Yield stress	0.09026	GPa
Ultimate tensile stress	0.175	GPa
Failure plastic strain = 0.75	0.75	–
Poisson's ratio	0.33	–

Due to its low specific weight, aluminum 6063–T6 alloy was selected and defined as the material for the module case model, thereby reducing the total weight of the battery (assembly thickness, 4 mm; density, 2.7 g/cm<sup>3</sup>; Poisson’s ratio, 0.33; Young’s modulus, 70 GPa).

### 3. Results and Discussion

The results obtained from the comparative numerical analysis of the effect of the implementation of auxetic elements in the structure of a battery are presented in this section by analyzing the following parameters: deformation, von Mises stresses, and energy variation during the impact process. The von Mises stress concentration plot on the battery case assembly provide a visualization of the deformation of the parts. The maximum stress is generated in the impact area.

Figure 7a shows the von Mises stress concentration of the assembly cell pack after impact with the rigid pole. The most significant deformations are in the battery pack and the rigid pole area, and the maximum von Mises stress value is  $5.193 \times 10^{-1}$  GPa. The energy curves are plotted after rigid pole impact analysis, as shown in Figure 7b. As can be seen, the kinetic energy curve starts from an initial value of 5197.50 J and remains constant for the first 1.77 ms. During this time, the battery pack assembly contacts the rigid pole. The kinetic energy curve drops continuously until 10.75 ms, and the level is close to zero. After the kinetic energy is completely absorbed in the battery pack, plastic deformation is converted into internal energy, and the deformation of the parts stops. Another aspect of this study is the maximum displacement resulting after impact. The largest displacements are in the contact area between the battery pack and the pole, as seen in Figure 7c. The maximum value of displacements is  $8.825 \times 10^1$  mm. According to the results of deformations (Figure 7d), the most affected area is in the middle of the assembly pack, where four rows of battery cells are destroyed. A summary of the damage caused by the crash shows that the heat exchanger structure was also destroyed. In this case, the cylinder energy absorbers absorb the kinetic energy to a small extent. The most energy is absorbed by the absorber in the contact area; after that, the cylindrical elements are placed on the opposite side of the impact, and the first two elements on the assembly side take over impact energy.

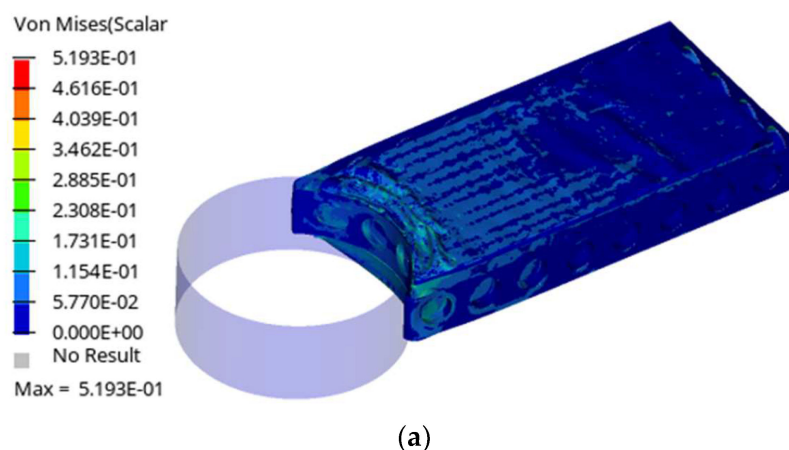
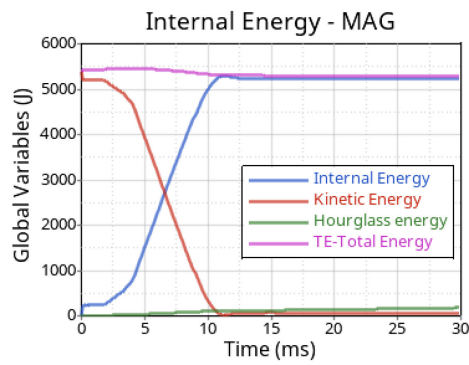
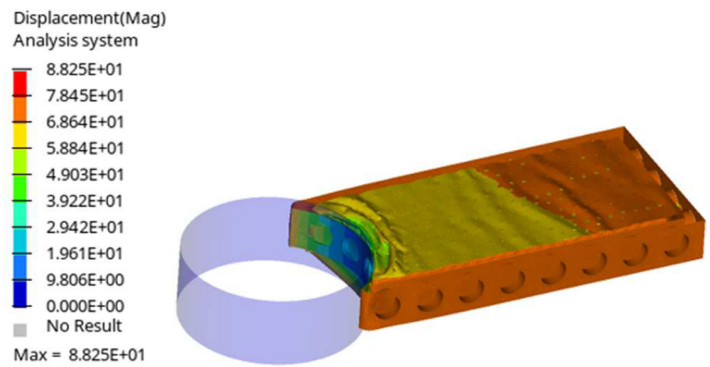


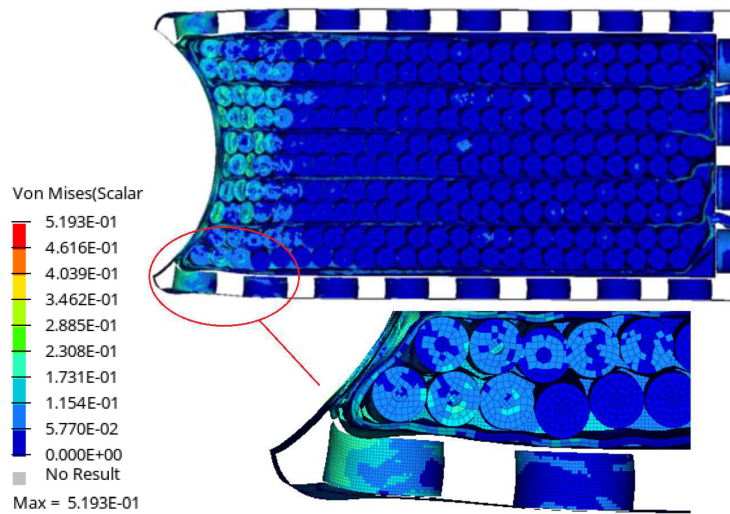
Figure 7. Cont.



(b)



(c)



(d)

**Figure 7.** Details of the effects of displacement, mechanical stress, and energy balance on modules and base cylindrical elements (CYL1) at a 10 m/s impact velocity ((a) von Mises stress; (b) energy balance; (c) displacement; (d) top view of the von Mises stress).

Figure 8a presents the von Mises stress concentration of the battery pack using the energy absorber with re-entrant perforation, with a maximum value of 1.337 GPa. After impact, the stress is distributed more evenly over the surface of the cell-fixing plate.

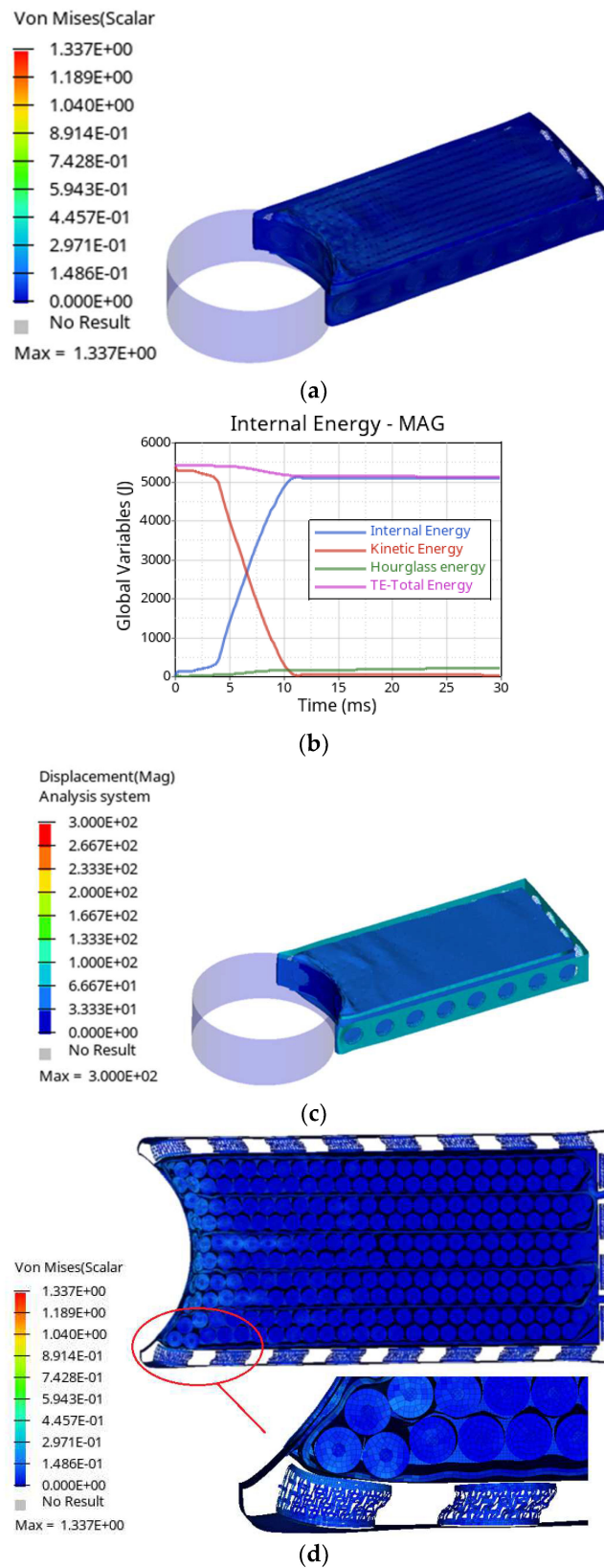


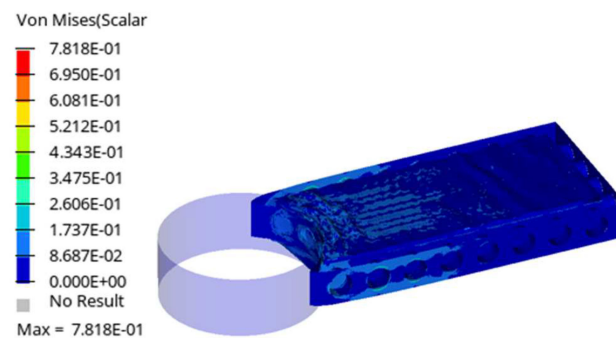
**Figure 8.** Details of the effects of displacement, mechanical stress, and energy balance on modules and re-entrant auxetic cylindrical elements (AUX1) at a 10 m/s impact velocity ((a) von Mises stress; (b) energy balance; (c) displacement; (d) top view of the von Mises stress).

The kinetic energy curve starts from a beginning value of 5260.50 J after remaining constant for the first 2.56 ms, as presented in Figure 8b. This value remains constant until the end of the experiment. The battery pack assembly hits the rigid pole at this time. After 10.23 ms, the level approaches zero, and the kinetic energy curve continues its steady decline until it stops.

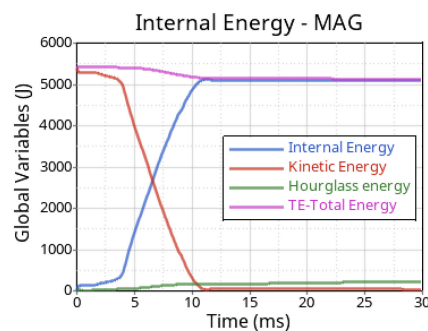
The maximum displacement distribution is presented in Figure 8c, where the value is  $3.000 \times 10^2$  mm, which is higher than in the previous case because the energy absorbers are more deformed than the base absorber, meaning more impact energy is absorbed by the auxetic structures.

The first two rows of battery cells are destroyed, and the third-row battery cells are partially affected by the crash impact. All cylindrical (auxetic) re-entrant energy absorber elements represent the active parts when taking charge of impact energy.

Figure 9 presents the results obtained in the second case of this study. The value of the maximum stress distribution in the assembly is  $7.818 \times 10^{-1}$  GPa, as represented in Figure 9a. The kinetic energy curve starts from an initial energy value of 5286.72 J (Figure 9b) and decreases slowly for the first 3.9 ms until 5006.75 J; then, the kinetic energy drops continuously until 11.16 ms. The maximum resulting displacement value in this case is  $8.602 \times 10^1$  mm. Figure 9c shows that a more considerable deformation is transmitted to the battery cell fixed between the plates and the heat exchanger. Figure 9d shows the first three destroyed rows of battery cells in the middle of the pack. The adjacent cells are less affected in the first two rows of the battery cells. In this case, the cylindrical parts absorb the kinetic energy from the impact area and gradually move to the four side parts.

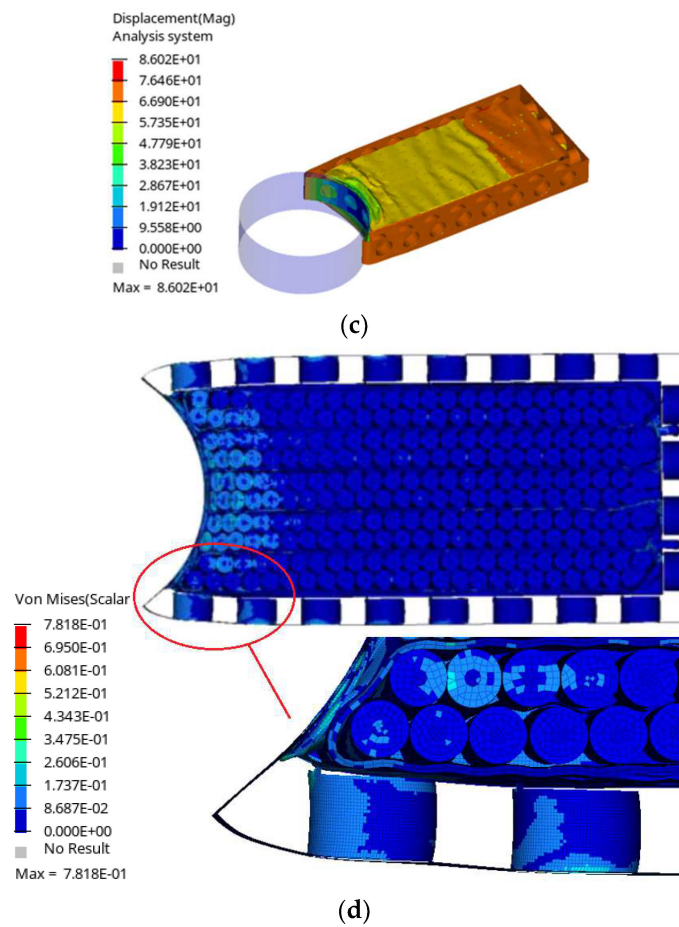


(a)



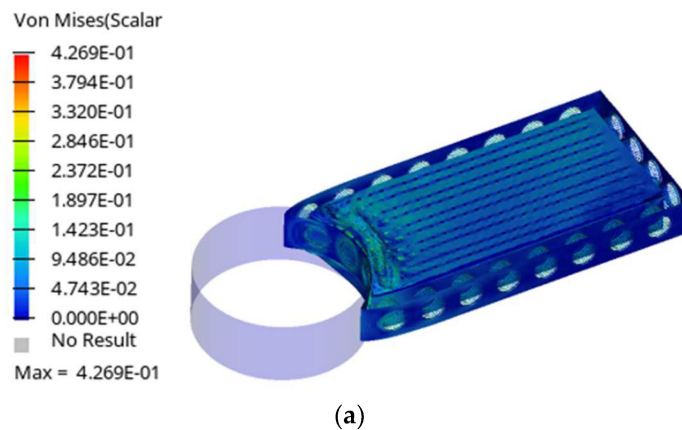
(b)

Figure 9. Cont.



**Figure 9.** Details of the effects of displacement, mechanical stress, and energy balance on modules and base cylindrical elements (CYL2) at a 10 m/s impact velocity ((a) von Mises stress; (b) energy balance; (c) displacement; (d) top view of the von Mises stress).

Figure 10a shows the crash results between the assembly cell pack, the rigid pole, and the von Mises stress. The maximum value of the von Mises stress concentration on the assembly pack is  $4.269 \times 10^{-1}$  GPa. As shown in Figure 10b, the kinetic energy curves start from an initial value of 5124.23 J, remaining constant for the first 3.2 ms. After that time, the energy curves decrease until 10.45 ms.



**Figure 10.** Cont.

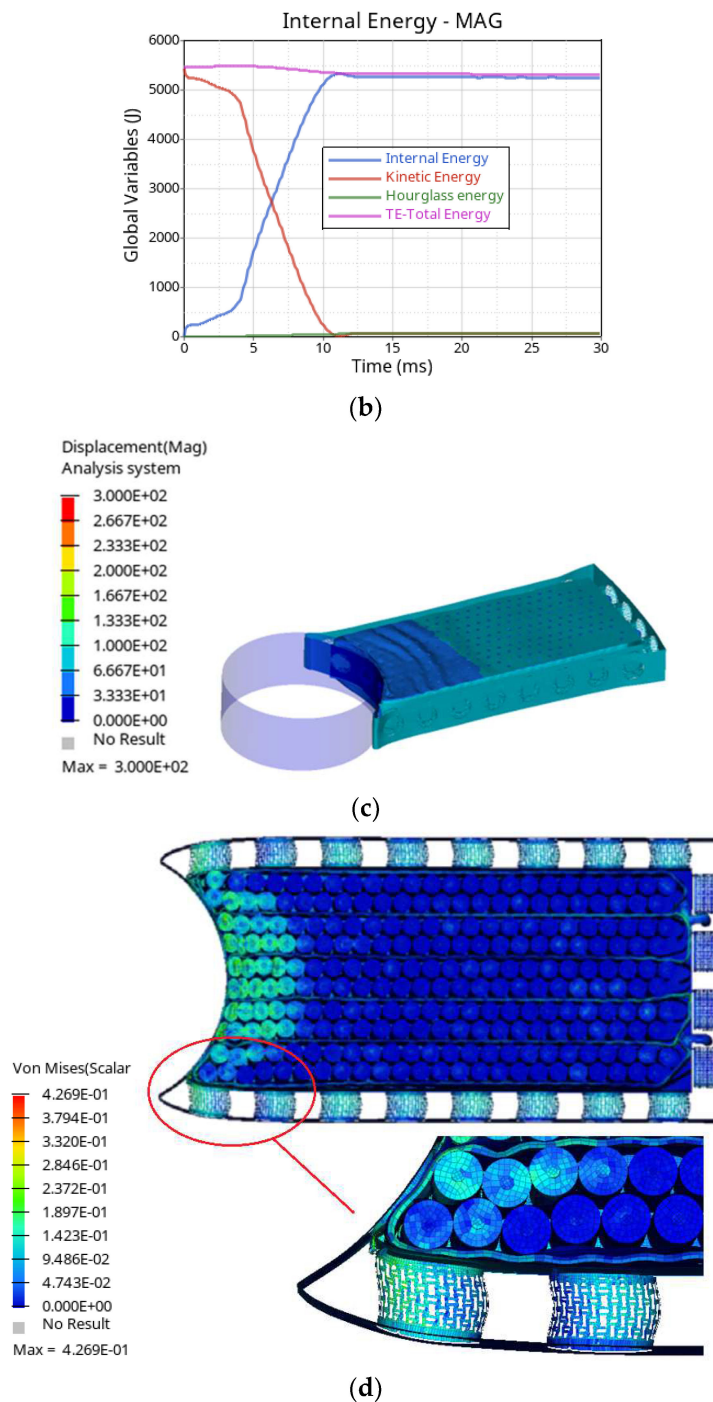
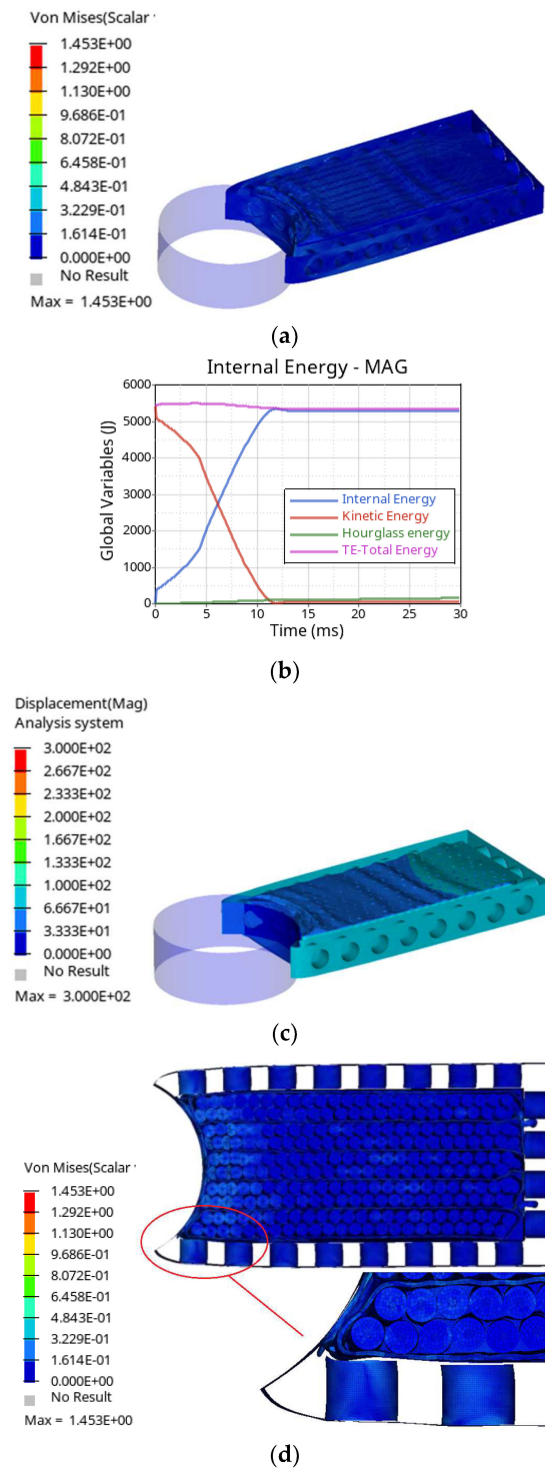


**Figure 10.** Details of the effects of displacement, mechanical stress, and energy balance on modules and re-entrant auxetic cylindrical elements (AUX2) at a 10 m/s impact velocity ((a) von Mises stress; (b) energy balance; (c) displacement; (d) top view of the von Mises stress).

The maximum displacement value observed in Figure 10c is  $3.000 \times 10^2$  mm and illustrates the propagation of a significant deformation in the battery cell fixed between the plate structure and the heat exchanger. The re-entrant side energy absorber elements can effectively dissipate the kinetic energy, as can be discerned from Figure 10d.

In the third case of this study (Figure 11a), the maximum value of von Mises stress concentration is  $1.453 \times 10^0$  GPa, with the fixing plates more deformed after impact. After impact, the heat exchanger and the four rows of battery cells in the middle of the battery pack are destroyed. The energy curve starts from an initial value of 5093.46 J, as seen in

Figure 11b, and after dropping continuously until 12.02 ms, the level is close to zero. Once the battery pack has fully absorbed the kinetic energy, the resulting plastic deformation is converted into internal energy, causing the deformation of the components to end. Another aspect evaluated in this study is the maximum displacement due to the impact, as shown in Figure 11c.



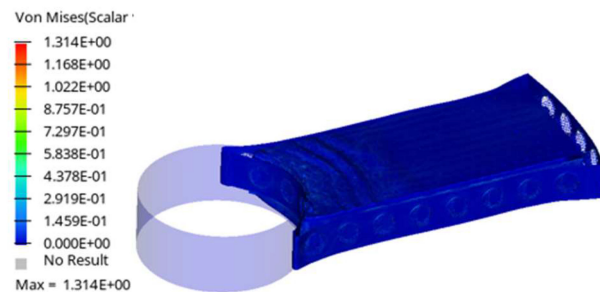
**Figure 11.** Details of the effects of displacement, mechanical stress, and energy balance on modules and base cylindrical elements (CYL3) at a 10 m/s impact velocity ((a) von Mises stress; (b) energy balance; (c) displacement; (d) top view of the von Mises stress).

Figure 11d shows that the first side energy absorbers are partially deformed, which shows that the absorber does not take over the kinetic energy.

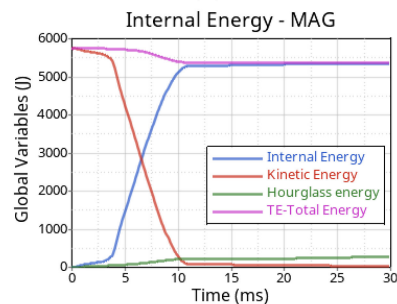
The last case in this study is presented as an analysis of the crash impact between the battery pack with an auxetic energy absorber and the rigid pole. The maximum value of the von Mises stress concentration is  $1.314 \times 10^0$  GPa, as presented in Figure 12a. As in the case of base energy absorber elements, the maximum displacement value of the battery case is  $3.000 \times 10^2$  mm. The kinetic energy starts at an initial value of 5812.95 J, as shown in Figure 12b, then gradually drops until reaching a value near zero at 11.28 ms. The result represented in Figure 12c shows a maximum displacement value of  $3.000 \times 10^2$  mm.

Figure 12d shows that the impact is higher in the present case, and the first battery cell rows are affected in the middle of the battery pack. In this case, the auxetic energy absorbed element takes over the kinetic energy.

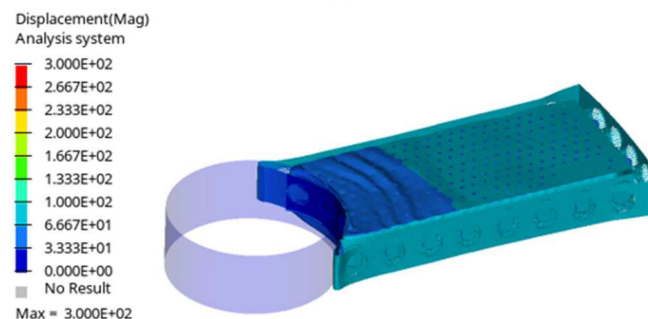
Simulation results show that the length of auxetic energy absorber cylinders influences their ability to deflect and absorb kinetic energy, with more extended absorber components exhibiting superior kinetic energy absorption capabilities. According to the validation of the simulation process, the total energy of the assembly remains constant during the impact.



(a)



(b)



(c)

Figure 12. Cont.

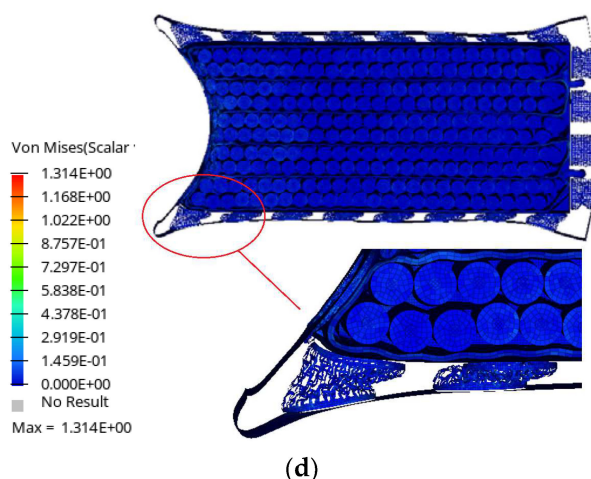


**Figure 12.** Details of the effects of displacement, mechanical stress, and energy balance on re-entrant auxetic cylindrical elements (AUX3) at a 10 m/s impact velocity ((a) von Mises stress; (b) energy balance; (c) displacement; (d) top view of the von Mises stress).

#### 4. Conclusions

As the demand for electric vehicles continues to grow, it is essential that manufacturers prioritize safety in operation (implicitly, battery impact protection) and therefore propose innovative solutions to meet these basic requirements.

This study focused on assembling energy absorption elements so that, in the event of an impact, they collectively absorb the energy of the effect. However, for the assembly to be as complete as possible in terms of geometry and for its impact behavior to be as accurate as possible, composite elements were introduced in the battery case.

This study simulated and evaluated the mechanical behavior of a battery case with auxetic structures included in its construction. Due to their distinct ability to respond elastically to mechanical shock, auxetic materials are ideally suited for mechanical shock absorption applications. This research is based on numerical analysis and considered an auxetic structure developed on various geometric dimensions (the considered variable was the height of the auxetic structure). The auxetic structure adjacent to the battery case retains the energy according to evaluation and comparison of the considered auxetic forms. It propagates around it, making it more resistant to impact and deformation.

To analyze the effectiveness of auxetic structures in reducing the mechanical impact demands on the battery, mechanical deformation suffered by the battery cells was considered as a comparison element. Through studies and experimental tests, the maximum value of the deformation up to which a cell can still be considered functional was determined to be 2.5 mm, and up to this value, the battery can be used safely without presenting risks [32].

In the case of the AUX1 auxetic structure, after simulations, 17 batteries had a deformation more significant than 2.5 mm. During the simulation performed on the AUX2 auxetic structure configuration, 15 individual cells of the 18,650 types had a mechanical deformation more significant than 2.5 mm. Based on the results, the optimal simulated model has auxetic elements (AUX3) with a length of 31 mm. In this case, the auxetic elements attenuate and absorb the kinetic energy during the impact. The number of affected individual cells is 11 pcs. The protection efficiency of the cells that make up the battery is 35.2% for the AUX3 structure compared to the AUX1 structure.

The longer the auxetic structure, the more efficient the transmission of energy from the front of the battery case to the sides. However, the major disadvantage is that in this case, the overall geometric and volume dimensions of the battery increase. A future direction of research would be to establish the optimal minimum dimensions of the auxetic structures (depending on the maximum impact value) that would provide the transfer of the frontal impact energy to other structural areas of the battery. Future comparative research needs to be carried out for other types of auxetic structures that can offer improved performance

in terms of absorbing mechanical shocks and protecting the battery cells (modules). Also, based on the already proposed and used auxetic structures, using shape optimization algorithms, new auxetic shapes can be developed and applied for the protection of electric vehicle batteries upon impact.

In this study, a velocity of 10 m/s was because most accidents occur at this velocity, in addition to the feasibility of using auxetic structures. It is the first step in a more complex study with different velocities and auxetic structures.

Given that, at least at the European level, there are requirements to increase the degree of recycling and recovery of components that form a battery, using auxetic elements may reduce the negative effects caused by mechanical stresses due to car accidents.

The novelty of this study is its new perspective and original insights. Its compelling arguments and well-researched facts stand out from other articles on the same topic. A successful reduction in impact energy and efficient transmission along the battery case were achieved by integrating auxetic structures into the fabrication of battery cases.

**Author Contributions:** Conceptualization, L.I.S. and I.S.; methodology, I.S. and M.G.; validation, L.I.S. and I.S.; formal analysis, I.S., L.I.S. and M.G.; investigation, L.I.S. and I.S.; writing—original draft preparation, I.S., L.I.S. and M.G.; writing—review and editing, L.I.S. and I.S. All authors have read and agreed to the published version of the manuscript.

**Funding:** This research received no external funding.

**Data Availability Statement:** Not applicable.

**Acknowledgments:** The authors express their gratitude to the Technical University of Cluj-Napoca for the financial support of the publication of this article.

**Conflicts of Interest:** The authors declare no conflict of interest.

## References

1. Lu, D.; Hu, D.; Yi, F.; Li, J.; Yang, Q. Optimal selection range of FCV power battery capacity considering the synergistic decay of dual power source lifespan. *Int. J. Hydrogen Energy* **2023**, *48*, 13578–13590. [[CrossRef](#)]
2. Jia, C.; Zhou, J.; He, H.; Li, J.; Wei, Z.; Li, K.; Shi, M. A novel energy management strategy for hybrid electric bus with fuel cell health and battery thermal- and health-constrained awareness. *Energy* **2023**, *271*, 7105. [[CrossRef](#)]
3. Zhou, J.; Feng, C.; Su, Q.; Jiang, S.; Fan, Z.; Ruan, J.; Sun, S.; Hu, L. The Multi-Objective Optimization of Powertrain Design and Energy Management Strategy for Fuel Cell–Battery Electric Vehicle. *Sustainability* **2022**, *14*, 6320. [[CrossRef](#)]
4. Shaddick, G.; Thomas, M.L.; Mudu, P.; Ruggeri, G.; Gumy, S. Half the world’s population are exposed to increasing air pollution. *NPJ Clim. Atmos. Sci.* **2020**, *3*, 23. [[CrossRef](#)]
5. Brătucu, G.; Trifan, A.; Dovleac, L.; Chițu, I.B.; Todor, R.D.; Brătucu, R. Acquisition of Electric Vehicles—A Step towards Green Consumption. Empirical Research among Romanian Students. *Sustainability* **2019**, *11*, 6639. [[CrossRef](#)]
6. Fuller, R.; Landrigan, P.J.; Balakrishnan, K.; Bathan, G.; Bose-O’Reilly, S.; Brauer, M.; Caravanos, J.; Chiles, T.; Cohen, A.; Corra, L.; et al. Pollution and health: A progress update. *Lancet Planet. Health* **2022**, *6*, e535–e547. [[CrossRef](#)] [[PubMed](#)]
7. Kukreja, J.; Nguyen, T.; Siegmund, T.; Chen, W.; Tsutsui, W.; Balakrishnan, K.; Liao, H.; Parab, N. Crash analysis of a conceptual electric vehicle with a damage tolerant battery pack. *Extrem. Mech. Lett.* **2016**, *9*, 371–378. [[CrossRef](#)]
8. Zhu, M.; Yang, H.; Liu, C.; Pu, Z.; Wang, Y. Real-time crash identification using connected electric vehicle operation data. *Accid. Anal. Prev.* **2022**, *173*, 106708. [[CrossRef](#)]
9. Gong, C.; Liu, J.; Han, Y.; Hu, Y.; Yu, H.; Zeng, R. Safety of Electric Vehicles in Crash Conditions: A Review of Hazards to Occupants, Regulatory Activities, and Technical Support. *IEEE Trans. Transp. Electr.* **2021**, *8*, 3870–3883. [[CrossRef](#)]
10. Liu, C.; Zhao, L.; Lu, C. Exploration of the characteristics and trends of electric vehicle crashes: A case study in Norway. *Eur. Transp. Res. Rev.* **2022**, *14*, 6. [[CrossRef](#)]
11. Shao, J.; Lin, C.; Yan, T.; Qi, C.; Hu, Y. Safety Characteristics of Lithium-Ion Batteries under Dynamic Impact Conditions. *Energies* **2022**, *15*, 9148. [[CrossRef](#)]
12. Belingardi, G.; Scattina, A. Battery Pack and Underbody: Integration in the Structure Design for Battery Electric Vehicles—Challenges and Solutions. *Vehicles* **2023**, *5*, 498–514. [[CrossRef](#)]
13. Carakapurwa, F.E.; Santosa, S.P. Design Optimization of Auxetic Structure for Crashworthy Pouch Battery Protection Using Machine Learning Method. *Energies* **2022**, *15*, 8404. [[CrossRef](#)]
14. Huo, S.; Gao, Z.; Ruan, D. Crashworthiness of a hybrid tube with an auxetic layer. *Eng. Fail. Anal.* **2022**, *142*, 106755. [[CrossRef](#)]
15. Vyavahare, S.; Kumar, S. Numerical and experimental investigation of FDM fabricated re-entrant auxetic structures of ABS and PLA materials under compressive loading. *Rapid Prototyp. J.* **2021**, *27*, 223–244. [[CrossRef](#)]

16. Photiou, D.; Avraam, S.; Sillani, F.; Verga, F.; Jay, O.; Papadakis, L. Experimental and Numerical Analysis of 3D Printed Polymer Tetra-Petal Auxetic Structures under Compression. *Appl. Sci.* **2021**, *11*, 10362. [[CrossRef](#)]
17. Veerabagu, U.; Palza, H.; Quero, F. Review: Auxetic Polymer-Based Mechanical Metamaterials for Biomedical Applications. *ACS Biomater. Sci. Eng.* **2022**, *8*, 2798–2824. [[CrossRef](#)] [[PubMed](#)]
18. Shirzad, M.; Zolfagharian, A.; Bodaghi, M.; Nam, S.Y. Auxetic metamaterials for bone-implanted medical devices: Recent advances and new perspectives. *Eur. J. Mech. A Solids* **2023**, *98*, 104905. [[CrossRef](#)]
19. Lvov, V.A.; Senatov, F.S.; Veeris, A.A.; Skrybykina, V.A.; Lantada, A.D. Auxetic Metamaterials for Biomedical Devices: Current Situation, Main Challenges, and Research Trends. *Materials* **2022**, *15*, 1439. [[CrossRef](#)]
20. Liu, Q. *Literature Review: Materials with Negative Poisson's Ratios and Potential Applications to Aerospace and Defence*; Australian Government Department of Defence: Canberra, Australia, 2006.
21. Shukla, S.; Behera, B. Auxetic fibrous structures and their composites: A review. *Compos. Struct.* **2022**, *290*, 115530. [[CrossRef](#)]
22. Alam Shah, I.; Khan, R.; Kooloor, S.S.R.; Petru, M.; Badshah, S.; Ahmad, S.; Amjad, M. Finite Element Analysis of the Ballistic Impact on Auxetic Sandwich Composite Human Body Armor. *Materials* **2022**, *15*, 2064. [[CrossRef](#)] [[PubMed](#)]
23. Junio, R.F.P.; da Silveira, P.H.P.M.; Neuba, L.d.M.; Monteiro, S.N.; Nascimento, L.F.C. Development and Applications of 3D Printing-Processed Auxetic Structures for High-Velocity Impact Protection: A Review. *Eng* **2023**, *4*, 903–940. [[CrossRef](#)]
24. Magalhaes, R.; Subramani, P.; Lisner, T.; Rana, S.; Ghiassi, B.; Fangueiro, R.; Oliveira, D.V.; Lourenco, P.B. Development, characterization and analysis of auxetic structures from braided composites and study the influence of material and structural parameters. *Compos. Part A Appl. Sci. Manuf.* **2016**, *87*, 86–97. [[CrossRef](#)]
25. Zahra, T. Role of auxetic composites in protection of building materials and structures. In Proceedings of the 9th International Advances in Applied Physics and Materials Science Congress and Exhibition, Mugla, Turkey, 22–28 October 2019.
26. Duncan, O.; Shepherd, T.; Moroney, C.; Foster, L.; Venkatraman, P.D.; Winwood, K.; Allen, T.; Alderson, A. Review of Auxetic Materials for Sports Applications: Expanding Options in Comfort and Protection. *Appl. Sci.* **2018**, *8*, 941. [[CrossRef](#)]
27. Moroney, C.; Alderson, A.; Allen, T.; Sanami, M.; Venkatraman, P. The Application of Auxetic Material for Protective Sports Apparel. *Proceedings* **2018**, *2*, 251. [[CrossRef](#)]
28. Luo, C.; Han, C.Z.; Zhang, X.Y.; Zhang, X.G.; Ren, X.; Xie, Y.M. Design, manufacturing and applications of auxetic tubular structures: A review. *Thin-Walled Struct.* **2021**, *163*, 107682. [[CrossRef](#)]
29. Wang, Z.; Luan, C.; Liaom, G.; Liu, J.; Yao, X.; Fu, J. Progress in Auxetic Mechanical Metamaterials: Structures, Characteristics, Manufacturing Methods, and Applications. *Adv. Eng. Mater.* **2020**, *22*, 2000312. [[CrossRef](#)]
30. Gunaydin, K.; Turkmen, H.S. In-Plane Quasi-Static Crushing Finite Element Analysis of Auxetic Lattices. In Proceedings of the 9th International Conference on Recent Advances in Space Technologies, RAST 2019, Istanbul, Turkey, 11–14 June 2019; pp. 645–648. [[CrossRef](#)]
31. Abdullah, N.; Sani, M.; Salwani, M.; Husain, N. A review on crashworthiness studies of crash box structure. *Thin Walled Struct.* **2020**, *153*, 106795. [[CrossRef](#)]
32. Biharta, M.A.S.; Santosa, S.P.; Widagdo, D.; Gunawan, L. Design and Optimization of Lightweight Lithium-Ion Battery Protector with 3D Auxetic Meta Structures. *World Electr. Veh. J.* **2022**, *13*, 118. [[CrossRef](#)]
33. Biharta, M.A.S.; Santosa, S.P.; Widagdo, D. Design and optimization of lithium-ion battery protector with auxetic honeycomb for in-plane impact using machine learning method. *Front. Energy Res.* **2023**, *11*, 1114263. [[CrossRef](#)]
34. Wang, W.; Dai, S.; Zhao, W.; Wang, C.; Ma, T. Design optimization of a novel negative Poisson's ratio non-module battery pack system considering crashworthiness and heat dissipation. *Compos. Struct.* **2021**, *275*, 114458. [[CrossRef](#)]

**Disclaimer/Publisher's Note:** The statements, opinions and data contained in all publications are solely those of the individual author(s) and contributor(s) and not of MDPI and/or the editor(s). MDPI and/or the editor(s) disclaim responsibility for any injury to people or property resulting from any ideas, methods, instructions or products referred to in the content.